Automated Image Analysis to Map the Extent of Deep-Sea Mining Plumes Reveals a Larger Impacted Area Compared to Manual Analysis

Timm Schoening (tschoening@geomar.de)
GEOMAR Helmholtz Centre for Ocean Research
Yasemin Bodur
UiT – the Arctic University of Norway
Kevin Köser
GEOMAR Helmholtz Centre for Ocean Research

Research Article

Keywords: poly-metallic nodules, blanketing, Terabytes, deep-sea mining, sediment plume

Posted Date: December 21st, 2021

DOI: https://doi.org/10.21203/rs.3.rs-1173923/v1

Abstract

Deep sea mining for poly-metallic nodules impacts the environment in many ways. A key potential hazard is the creation of a sediment plume from resuspending sediment during seabed mining. The resuspended matter disperses with currents but eventually resettles on the seabed. Resettling causes a blanketing of the seafloor environment, potentially causing harm to in-, epi- and hyperbenthic communities with possible cascading effects into food webs of deep sea habitats. Mapping the extent of such blanketing is thus an important factor in quantifying potential impacts of deep-sea mining.

One technology that can assess seabed blanketing is optical imaging with cameras at square-kilometre scale. To efficiently analyse the resulting Terabytes of image data with minimized bias, automated image analysis is required. Moreover, effective quantitative monitoring of the blanketing requires ground truthing of the image data. Here, we present results from a camera-based monitoring of a deep-sea mining simulation combined with automated image analysis using the CoMoNoD method and low-cost seabed sediment traps for quantification of the blanketing thickness. We found that the impacted area was about 50 percent larger than previously determined by manual image annotation.

Introduction

Poly-metallic nodules are one of the three seafloor mineral deposits currently under exploration for deep-sea mining[1]. Their metal content is controversially discussed as a solution to metal shortages by a growing economy and the green revolution[1]. Nodules occur over millions of square kilometres, e.g. in the Clarion-Clipperton Fracture Zone (CCZ) in the Pacific Ocean. They lie embedded in the seafloor sediment, with Gigatons visible at the seafloor[2] and unknown amounts buried. In the CCZ, natural sedimentation rates are below 1 cm per 1000 years[2].

The current state-of-the-art in mining technology is still in a prototype stage, yet a disturbance of the seafloor sediments by the mining gear is expected[3]. This disturbance will create a plume of resuspended sediment that will rise to an unknown altitude up from the seafloor and will also migrate laterally with currents[4]. While some material may dissolve in the water column, most of the resuspended particulate matter will resettle at the seafloor[5]. This resettling will likely occur some distance away from the mining disturbance[4]. Past seafloor mining simulations and disturbance experiments have shown sediment resettlement at a distance of several hundreds of meters away from the disturbance, even at the small scale of those simulations when compared to the expected impacts of industrial deep-sea mining activities[6].

Amongst other mining-induced impacts, the plume itself and the blanketing caused by its resettling are expected to negatively affect the fragile deep-sea habitat[7]. To date, the scale of all impacts and their effects are poorly understood. International research projects aim to quantify gradients and thresholds of various impacts across scales[8]. Such thresholds are urgently needed to shape the mining code currently

in preparation by the International Seabed Authority[9]. Based on this mining code, contractors and mining companies will be obliged to monitor their activity to prevent unnecessary harm to the environment.

To effectively monitor plume distribution, sensor arrays to measure suspended particles are required – like turbidity meters and Doppler current velocimeters with backscatter information[10]. To effectively monitor the extent and thickness of the blanketing of the seafloor, extensive mapping is required[6]. Acoustic mapping can create overview maps of nodule fields and enables efficient assessment of severe sediment re-depositing. Those maps do however not allow the exact quantification of seafloor blanketing and cannot discover thin layers of blanketing below 1 mm sediment coverage. But even such thin layers and low concentrations are expected to have adverse and potentially lethal effects on deep sea fauna. Consequently, the capacity to monitor their extent is necessary to monitor deep-sea mining[11]. Assuming that deep-sea mining will only be conducted at high environmental protection standards, such mapping is in turn also required to facilitate mining in general.

A proven technology to achieve such mapping at kilometre-scale effectively and efficiently, is optical imaging with cameras operated at close distance to the seafloor (1-10 meters)[12]. In such camera footage, individual nodules are visible, as are epibenthic megafauna, severe seafloor disturbances as well as faint seafloor blanketing[6]. That way, imaging solves several requirements for habitat baseline assessment, resource assessment and impact monitoring at once.

Extracting quantifiable information from the resulting Terabytes of images is the challenge that was often seen as a barrier to use imaging at large[13]. Manual image annotation has shown to be error-prone and labour-intense, although some mitigation recommendations have been proposed[14–16]. Still, with increasing amounts of autonomous robotic platforms creating exponentially increasing amounts of image data, only computational image analysis can solve this task. Several pattern recognition and AI methods have successfully been applied to seafloor image data sets to detect nodules and deep-sea fauna[17–19]. By imaging before and after a disturbance and comparing the detection results, plume distributions have already been assessed qualitatively[6]. Aside from the analysis speedup, automated image analysis also has the benefit of creating results that are not influenced by human bias[20].

Anyhow, the typical 2D image material can only provide a qualitative plume blanketing assessment. Imaging needs to be combined and calibrated with a direct measurement method to analyse blanketing (semi-)quantitatively. Such measurements can be obtained from sediment traps but those are costly to acquire, deploy and recover[21]. An array of multiple sediment traps would be needed per hectare, rendering this approach infeasible. Simple “ruler sticks” deployed pre-disturbance and surveyed post-disturbance can quantify blanketing at ca. centimetre resolution and thus for high sediment loads only. A key challenge for measurement is that even the order of magnitude of expected sediment depositing at a certain spot can be difficult to predict (sub-millimeter, sub-centimeter, sub-decimeter), and so specific instruments might quickly be saturated at one location or might not be sensitive enough at another

location. Consequently, a method is required that covers a high dynamic range, is easy to deploy, easy to read out, is robust and ideally affordable.

This study uses seafloor image data, automated image analysis and dedicated low-cost sediment traps (called “Sediment Level IndiCator” boxes) for low and high sediment loads to quantify the extent of blanketing caused by a deep-sea mining simulation. The combination of these methods allows to create a high-resolution map of the plume extent effectively and efficiently.

We found that the objective automated image analysis correctly determined an impacted seafloor area 50 percent larger when compared to the impacted area determined by at-sea ad-hoc manual image interpretation.

Methods

Mining simulation:

During cruise SO268, a sediment plume was created by repeatedly dredging the seafloor with an open dredge[8]. The same East-West extent was dredged several times while shifting the vessel southwards with each consecutive transect to create a ca. 450x50m large disturbance at the seafloor. Dredging created direct impacts at the seafloor such as dredge tracks, cable tracks and sediment displacements as well as indirect impacts due to sediment lumps having fallen off the dredge during hoisting and the resettling of the sediment plume. Example images of the dredge impacts are given in Figure 1.

OFOS imaging:

Image data was acquired by the OFOS of RV Sonne[8]. The system consists of a steel frame with one still image camera and one HD video camera and was run with USBL positioning. The OFOS was maintained and operated by the crew of RV Sonne. It featured a heave-compensation that resulted in stable imaging conditions. The OFOS projected three laser pointers for scaling into the fields of view of both cameras.

Image data of both cameras was transmitted via fibre-optic cable up to the vessel and stored on dedicated hardware. Both feeds were available immediately for navigational control and scientific annotation. Four of the twelve OFOS deployments of cruise SO268 were conducted in the plume impact area. Deployment SO268/2_100-1 was conducted 5 days before creation of the plume. Deployments SO268/2_126-1, SO268/2_160-1 and SO268/2_164_1 were conducted 3, 17 and 18 days afterwards, respectively. The video feeds of all deployments were annotated live for fauna occurrences. The four plume-related deployments were annotated for plume impacts as well. All annotations were done with the OFOP software[22].

SLIC box blanketing thickness measurement:

As image data can only provide semi-quantitative data on blanketing thickness, direct measurements of that parameter were required by another method and at an informative sampling resolution. As traditional

sediment traps are too costly to acquire, deploy and recover[21], the concept of “Sediment Level IndiCator” (SLIC) boxes was developed prior to cruise SO268. SLIC boxes were designed as stackable steel frames to be deployed in groups of ten by ROV (see Figure 2). They consisted of two compartments of corrugated sheet of different wavelength and amplitude. This design was chosen to enable trapping of resettling sediment in the troughs of the corrugations. Focussing the sediment in the troughs of known shape allows laterally measuring the width of a sediment-covered area, rather than requiring a vertical depth measurement to quantify the volume of blanketing material. The goal was to image the SLIC boxes after a plume event from an altitude of 5 meters or more to measure blanketing thickness. The corrugations of the SLIC boxes were designed to quantify the expected plume blanketing for sediment loads of up to 1-5 cm thickness. For higher sediment loads an additional ruler stick of 30 cm length was added to the side of each SLIC box.

Thirteen SLIC boxes were correctly deployed by ROV and placed at distances up to 100 meters away from the planned dredge tracks. Due to wave state, seven SLIC boxes were lost during platform deployment and descent, of which two accidentally landed upright in the centre of the planned dredge area after free-falling through 4500m of water. One lost SLIC box was found 300 m south of the planned dredge tracks, outside of the target area for the sediment traps. All fifteen usable SLIC boxes were imaged by ROV before the dredging to assess the pre-disturbance sediment load baseline. After dredging, all SLIC boxes were imaged again.

CoMoNoD nodule detection:

Each OFOS still image was processed individually by the CoMoNoD algorithm to delineate each single nodule in each image[18]. Nodule delineation resulted in a size measurement of each nodule in pixels. To transform this measurement to a size in square centimetres, automated laser point detection was used to determine the millimetre-size of a pixel of each image separately[23]. Applying this conversion factor provided individual size measurements of nodules. To assess resource abundance, additional conversion factors to nodule weights would be needed but for plume mapping the computed size measurements suffice[24]. From individual nodule sizes, CoMoNoD computed the number of nodules per square meter, the seafloor coverage by nodules in percent and the median size of all nodules in an image. Furthermore, CoMoNoD computes factors for particle size distribution analysis which were not needed for this study.

Both the execution of the CoMoNoD algorithm and the automated laser point detection were executed on a mobile GPU compute cluster for at-sea high-performance computing[25].

Mapping the blanketing extent:

OFOS deployments normally result in image locations along transects. In this case, to map the plume extent, dynamic positioning of RV Sonne was used to criss-cross the area of expected plume impact. The goal was to facilitate a contiguous map by imaging closely together in adjacent lines. Still, gaps of up to 50 meters between imaging locations occurred. To compute a contiguous map, linear interpolation by the *scipy.interpolate.griddata* function was used. One interpolated map was computed for each CoMoNoD

parameter (i.e. nodules per square meter, seafloor coverage, median nodule size) and for the situation before and after the dredging. A difference image was then computed by subtracting the pre-dredging map of each parameter from its post-dredging map. This results in areas of negative values where pre-dredging measurements exceed post-dredging values. Each of these three difference images was then thresholded at the first turning point of the value histogram above the minimum value. The resulting outlines were interpreted as the extent of the measurable plume extent according to that parameter.

Results

The four OFOS deployments for plume monitoring resulted in a total of 12,908 still images[8]. Of those, 2,768 were acquired before the impact. The post-dredging images show a variety of impacts. See Figure 1 for example images of the undisturbed and disturbed seafloor.

Sediment loads in the SLIC boxes were much smaller than what the boxes were designed for as the seafloor disturbance itself was much smaller than what was planned for before the cruise. Hence, the sediment load of the SLIC boxes after the disturbance was below 1 cm in all cases. See Figure 2 for a comparison of before and after blanketing. Anyhow, sediment loads could be measured semi-quantitatively and were estimated >1 mm for the four SLIC boxes in the centre of dredging activity. Five SLIC boxes further South of the disturbance showed sediment loads <1 mm as well as two SLIC boxes North of the deployment. One of those was in close vicinity to the dredging, while one was located ca. 85 m upstream, likely showing a sediment load caused by simultaneous sampling activity rather than dredging. All other SLIC boxes upstream and the lost one 300 m south of the dredging showed no apparent change in sediment load after dredging.

Processing the still images with the CoMoNoD algorithm resulted in nodule delineations for each image which were combined to measures of median nodule size, nodule coverage of the seafloor and nodule number per square meter, all given per image analysed. The dredging had an obvious effect on the nodules detection results (see Figure 3). The median number of detected nodules per square meter decreased from 74.1 to 73.9; the median estimated nodule coverage decreased from 13 to 11 percent; the median nodule size decreased from 3.6 to 3.4 cm.

Manual video annotations were plotted on a map by USBL location to create a quick overview of the plume impact. This extent was correlated with the results from the SLIC boxes to outline the areas of more than 1 mm blanketing and visible blanketing of less than 1 mm (see Figure 4).

Automated image analysis provided three boundaries for impact extents, one for each of the three parameters CoMoNoD computes (see Figure 4, grey lines). The extent of the impacted area in terms of reduced nodule size and reduced nodule coverage overlaps by 83 percent. Hence, these two parameters were interpreted to quantify the same impact. When combining the CoMoNoD results with the SLIC numbers it was firstly apparent that the area of reduced nodule numbers detected shows sediment loads

>1 mm in the SLIC boxes. Secondly, SLIC boxes showing >0 yet <1 mm sediment load additionally occurred throughout the area of reduced nodule size and coverage.

It was concluded, that the CoMoNoD results for reduced nodule number detections correspond to the manual annotations of >1 mm blanketing. 86 percent of the annotated area overlap with the automatically computed area while that area is 27 percent larger than the annotated area. The area, where the coverage of nodules was apparently reduced, overlaps to the area annotated as >0 mm yet <1 mm blanketing at 87 percent despite the automatically computed area being 51 percent larger. The area, where the size of nodules was apparently reduced, overlaps to the area annotated as >0 mm yet <1 mm blanketing at 79 percent despite the automatically computed area being 54 percent larger.

Discussion

The larger extent of impacted area from CoMoNoD results largely coincides with two North-South-oriented depressions apparent in AUV bathymetry data. The western one of these two impact extensions reaches beyond the area imaged by OFOS. This results in the sharp cut-off of the grey lines visible towards the lower end of Figure 4. It is likely, that the impacted area extends beyond the surveyed area. This finding of extended blanketing along slopes is in line with other observations[6].

The partly overlapping results of manual and automated image analysis indicate that the human annotators were likely influenced in their annotation decisions by the visual representation of the parameters determined by the CoMoNoD algorithms. Anyhow, mapping the extent of the blanketing requires an objective method that is not influenced by tiredness, distraction, the person currently annotating or else. This was apparent in the CoMoNoD results that correctly determined areas showing blanketing outside of the areas determined by manual annotation. Relying on the manual interpretation would have underestimated the plume impact at the seafloor.

While the blanketing extent could be assessed, this method cannot quantify the suspended plume. Other works on an acoustic and optical sensor array are being published elsewhere to report on that aspect of this plume (Halboom et al., in review).

Additionally, the presented method only allows to quantify macroscopic effects and does not provide information on impacts on meio-, macro- or in-fauna.

This study was limited by several technical failures that altered the monitoring capability as well as the intended scope of the plume mapping exercise[8]. It was planned to monitor the first industry-scale deep-sea mining activity using the Patania II vehicle. Due to technical issues, this could not be achieved and the small-scale dredge plume simulation was executed instead. As a result, the remobilized sediment amounts were much lower than previously planned.

In addition, it was initially planned to conduct the imaging using an AUV. Unfortunately, this AUV also suffered technical failure, resulting in no recorded image data. Using the OFOS was the backup solution

and proved to be effective in creating the required data and results. Anyhow, an OFOS system cannot efficiently be deployed to monitor a contiguous area, resulting in excessive use of ship time to facilitate the mapping.

Due to the reduced amount of remobilized sediment, the plume simulation was undersized regarding the SLIC box design. The recorded blanketing of >1 mm, yet less than 1 cm, was outside of the initially planned scope of the low-cost sediment traps. It was also evident, that the corrugations were not steep or slippery enough to steer all particles to the bottom of the corrugation troughs. At the same time, the design using cheap corrugated sheet proved successful only in parts, as some sediment remained on top of the ridges of the corrugations. For a future design of low-cost blanketing quantification, we recommend to replace one of the corrugations with a saw tooth-style sheet that features straight slopes rather than the sigmoidal slopes of the corrugations. This will also ease the computation of redeposited sediment volumes. The corrugation from the other half of the SLIC boxes should be replaced by a flat checkerboard of black and white squares. Faint sediment blanketing can be assessed by inspecting color change. In addition, the checkerboard pattern enables highly-demanded in-situ camera calibration for increased accuracy for seafloor mosaicking or biomass measurements.

Manual live annotation for plume impacts can be achieved at real-time speed, in this case requiring 27 hours to complete. The results are affected by annotation bias though. Application of the CoMoNoD method resulted in objective blanketing maps with high efficiency. Computing the CoMoNoD results for individual images requires ca 15 minutes on a GPU compute cluster. The following map creation is an interactive process and achievable in less than 30 minutes.

To speed this process up even further, we are currently migrating the image analysis capability from the GPU cluster into a GPU compute-enabled camera system for edge computing. This will allow to compute – and acoustically transmit – nodule detection numbers to the sea surface live during deployments. This camera system should ideally be operated on an AUV but the technology can be deployed on other platforms as well. Similarly, the approach presented here can not only be applied to monitor mining impacts by plumes but can also be used to assess other seafloor plumes, e.g. created by benthic storms, landslides, submarine canyon downslope transport events. The prerequisite however is an extensive pre-disturbance image survey and the deployment of sediment traps for quantification.

Mapping the extent of plumes should be done by several AUVs. These platforms can effectively and efficiently monitor the spatial and temporal aspects of plume distribution. By operating turbidity meters and acoustic backscatter sensors on AUVs, the suspended plume can be mapped in 4D. By operating camera systems with GPU compute-capacity, seafloor blanketing can be measured in-situ. In combination with low-cost, or even disposable, sediment traps designed for image-based information retrieval, a tool set exists that can provide information on baselines, resource assessment and, most importantly, enables plume monitoring. Several AUVs should be operated in parallel to prevent critical technical failure by relying on a single platform and to further increase monitoring efficiency.

We recommend including extensive imaging with AUVs into the requirements for mining companies, both to enable baseline assessment as well as monitoring of active and past mining operations. Not only are images a valuable and credible information source for these use cases, but also inherently accessible and appealing to humans in fostering excitement and interest in ocean processes and ocean narratives. We hope, image data can also see and create an increased involvement in ocean governance.

This study adds another indication that mining-related impacts need to be quantified properly. Thorough reliability testing of all deep-sea mining monitoring methods must be achieved before mining activities may commence. A precautionary principle has to be applied in either case as all methods may suffer from unforeseen bias. Despite being a community standard, manual annotation did underestimate the impacted area by ca. fifty percent in this study. Future improvements in automated image analysis capacity may reveal an even larger impacted area with unknown effects to the deep-sea habitat.

Declarations

Data Availability

OFOS still image data is available on PANGAEA at https://doi.org/10.1594/PANGAEA.935856 and nodule detection results are available at https://doi.org/10.1594/PANGAEA.935231

Code Availability

The source code of the CoMoNoD method is available as part of the open source C++ library OceanCV: https://git.geomar.de/open-source/oceancv

Acknowledgements

We thank the crew of RV Sonne for their invaluable support during cruises SO268/1 and SO268/2. The quality of the onboard OFOS system and the capabilities of the technical, nautical and deck teams proved again to be outstanding. We also thank the ROV team of GEOMAR and the technicians of the SO268 science party for their support in acquiring the data used in this study. Many thanks also to Matthias Haeckel for creating the dredge plume and to the team of CCT1 of the MiningImpact project for their help on board. This work was financially supported by the JPI Oceans project MiningImpact “Environmental Impacts and Risks of Deep-Sea Mining” (FKZ: 03F0812A). KK received funding by the German Research Foundation (Deutsche Forschungsgemeinschaft, DFG) Projektnummer 396311425, through the Emmy Noether Programme. YB was supported by the BenthImpact project (FKZ: 03F0812D).

Author contributions

YB, TS and KK acquired the image data on board. KK and TS developed the SLIC box concept. TS, KK and YB wrote this manuscript.

Competing interests

The authors declare no competing interests.

References

1. Petersen, S. *et al.* News from the seabed – Geological characteristics and resource potential of deep-sea mineral resources. *Mar. Policy* **70**, 175–187 (2016).
2. Peukert, A., Petersen, S., Greinert, J. & Charlot, F. Seabed mining. in *Submarine Geomorphology* 481–502 (Springer, 2018).
3. Weaver, P. P. E. & Billett, D. Environmental impacts of nodule, crust and sulphide mining: an overview. *Environ. Issues Deep. Min.* 27–62 (2019).
4. Jones, D. O. B., Ardron, J. A., Colaço, A. & Durden, J. M. Environmental considerations for impact and preservation reference zones for deep-sea polymetallic nodule mining. *Mar. Policy* **118**, (2020).
5. Gillard, B. *et al.* Physical and hydrodynamic properties of deep sea mining-generated, abyssal sediment plumes in the Clarion Clipperton Fracture Zone (eastern-central Pacific). *Elem. Sci. Anthr.* **7**, (2019).
6. Peukert, A. *et al.* Understanding Mn-nodule distribution and evaluation of related deep-sea mining impacts using AUV-based hydroacoustic and optical data. *Biogeosciences* **15**, (2018).
7. Simon-Lledó, E. *et al.* Ecology of a polymetallic nodule occurrence gradient: Implications for deep-sea mining. *Limnol. Oceanogr.* **64**, (2019).
8. Haeckel, M. & Linke, P. *RV SONNE Fahrtbericht/Cruise Report SO268 - Assessing the Impacts of Nodule Mining on the Deep-sea Environment: NoduleMonitoring, Manzanillo (Mexico) ? Vancouver (Canada), 17.02. ? 27.05.2019*. **N**. **Ser**. **05**, (ARRAY(0xcfd1f1c), 2021).
9. Levin, L. A. *et al.* Defining “serious harm” to the marine environment in the context of deep-seabed mining. *Mar. Policy* **74**, 245–259 (2016).
10. Spearman, J. *et al.* Measurement and modelling of deep sea sediment plumes and implications for deep sea mining. *Sci. Rep.* **10**, 1–14 (2020).
11. Washburn, T. W. *et al.* Ecological risk assessment for deep-sea mining. *Ocean \& Coast. Manag.* **176**, 24–39 (2019).
12. Schoening, T., Köser, K. & Greinert, J. An acquisition, curation and management workflow for sustainable, terabyte-scale marine image analysis. *Sci. data* **5**, 1–12 (2018).
13. Durden, J. M. *et al.* Perspectives in visual imaging for marine biology and ecology: from acquisition to understanding. *Oceanogr. Mar. Biol. An Annu. Rev.* **54**, 1–72 (2016).

14. Schoening, T., Osterloff, J. & Nattkemper, T. W. RecoMIA—Recommendations for Marine Image Annotation: Lessons Learned and Future Directions. *Front. Mar. Sci.* **3**, 59 (2016).
15. Langenkämper, D., Zurowietz, M., Schoening, T. & Nattkemper, T. W. BIIGLE 2.0 - Browsing and Annotating Large Marine Image Collections. *Front. Mar. Sci.* **4**, 1–10 (2017).
16. Schoening, T. *et al.* Megafauna community assessment of polymetallic-nodule fields with cameras: platform and methodology comparison. *Biogeosciences* **17**, 3115–3133 (2020).
17. Schoening, T., Kuhn, T., Jones, D. O. B., Simon-Lledo, E. & Nattkemper, T. W. Fully automated image segmentation for benthic resource assessment of poly-metallic nodules. *Methods Oceanogr.* **15–16**, 78–89 (2016).
18. Schoening, T., Jones, D. O. B. & Greinert, J. Compact-Morphology-based poly-metallic Nodule Delineation.
19. Schoening, T. *et al.* Semi-automated image analysis for the assessment of megafaunal densities at the Artic deep-sea observatory HAUSGARTEN. *PLoS One* **7**, e38179 (2012).
20. Schoening, T., Bergmann, M. & Nattkemper, T. W. Investigation of hidden parameters influencing the automated object detection in images from the deep seafloor of the HAUSGARTEN observatory. in *OCEANS 2012 MTS/IEEE: Harnessing the Power of the Ocean* (2012). doi:10.1109/OCEANS.2012.6405040
21. de Stigter, H. C. *et al.* Recent sediment transport and deposition in the Nazaré Canyon, Portuguese continental margin. *Mar. Geol.* **246**, 144–164 (2007).
22. Gomes-Pereira, J. N. *et al.* Current and future trends in marine image annotation software. *Prog. Oceanogr.* **149**, 106–120 (2016).
23. Schoening, T. *et al.* Fast and adaptive computational laser point detection and visual footprint quantification for arbitrary underwater image collections. *Front. Mar. Sci.* **2**, (2015).
24. Schoening, T. & Gazis, I.-Z. Sizes, weights and volumes of poly-metallic nodules from box cores taken during SONNE cruises SO268/1 and SO268/2. (2019). doi:10.1594/PANGAEA.904962
25. Schoening, T. SHiPCC—A Sea-going High-Performance Compute Cluster for Image Analysis. *Front. Mar. Sci.* **6**, (2019).

Figures

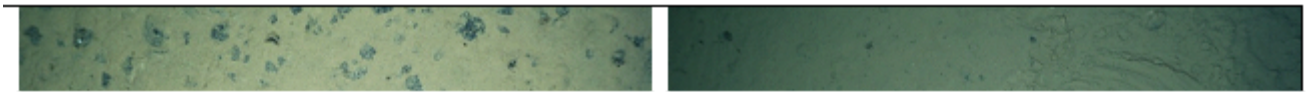

Figure 1

example seafloor images and impacts. Top left: undisturbed seafloor; top right: start of dredge track; bottom left: blanketing of <1 mm; bottom right: blanketing of >1 mm.

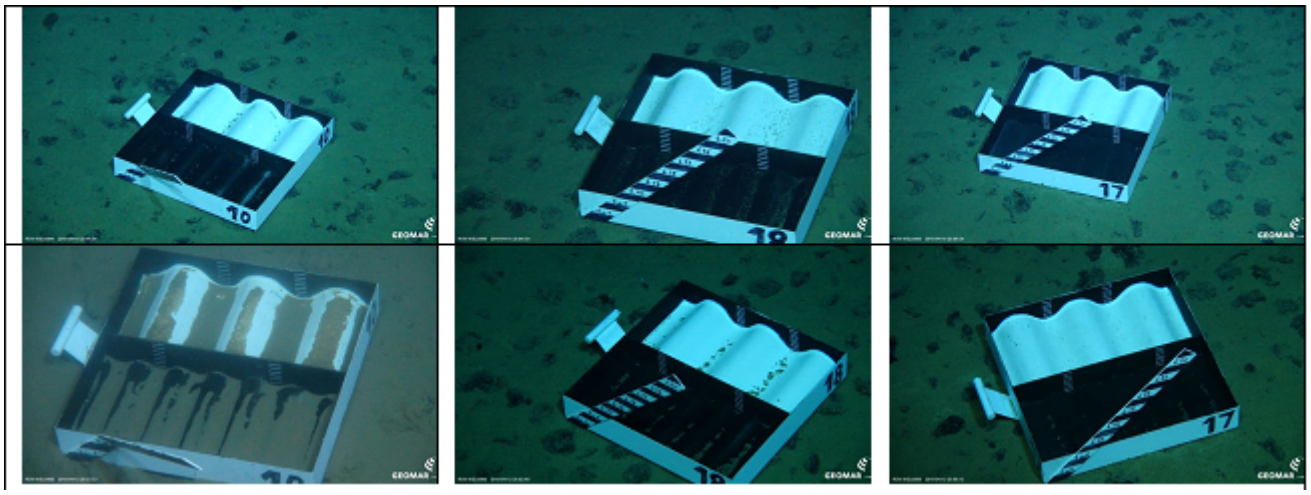

Figure 2

Selected SLIC box results showing conditions before (top) and after dredging (bottom) for the three conditions >1 mm blanketing (left), < 1 mm blanketing (middle) and no blanketing (right).

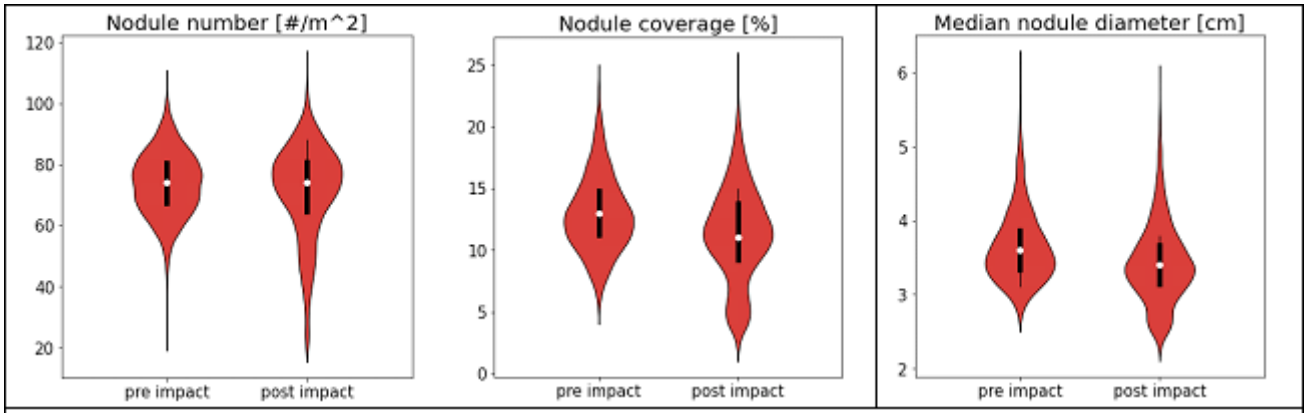

Figure 3

Violin plots of nodule statistics determined by CoMoNoD. All three parameter values decrease after the impact, indicating a blanketing in parts of the images.

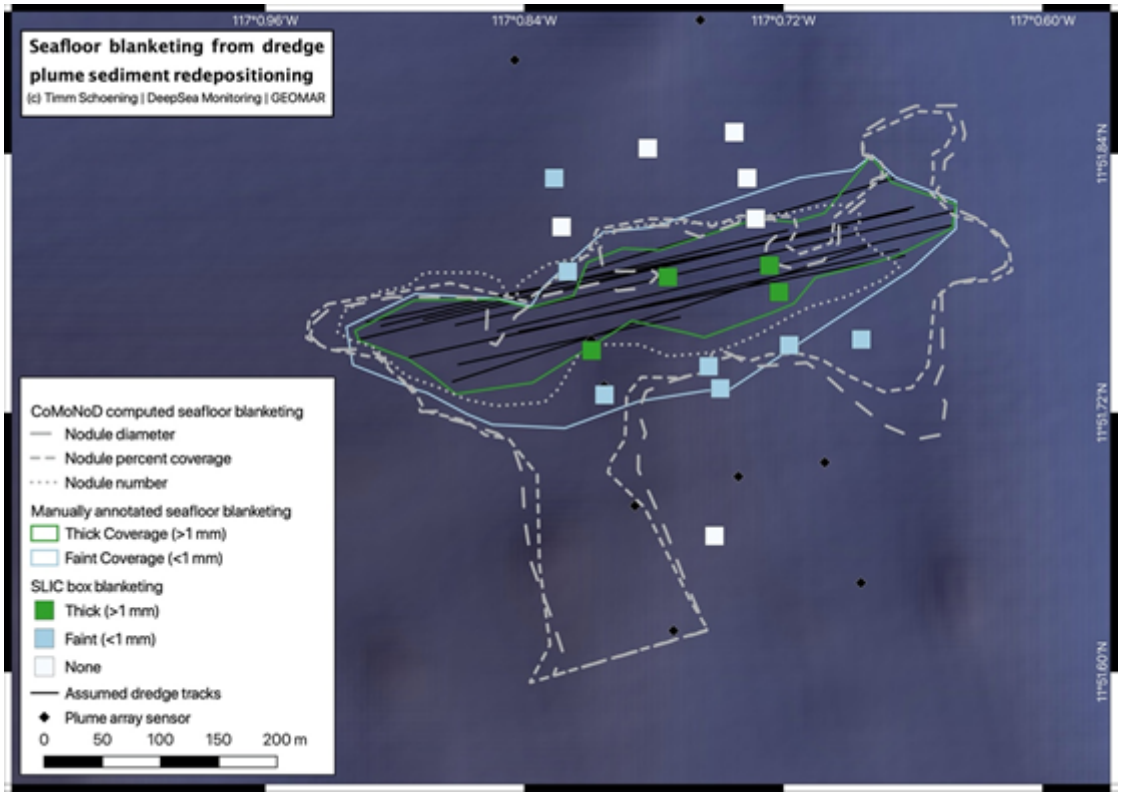

Figure 4

Seafloor blanketing extent mapped by manual (green and blue lines) and automated image analysis (grey lines). Different colors and line stiles correspond to different impact measures. Locations of SLIC boxes are given by colored squares.